JOURNAL OF MAGNETIC RESONANCE **131,** 97–110 (1998)
ARTICLE NO. MN971338

Determination of High-Spin Iron(III)–Nitroxyl Distances in Spin-Labeled Porphyrins by Time-Domain EPR

Margaret H. Rakowsky, Ana Zecevic, Gareth R. Eaton, and Sandra S. Eaton

Department of Chemistry and Biochemistry, University of Denver, Denver, Colorado 80208

Received April 24, 1997; revised November 6, 1997

Continuous wave EPR spectra of the nitroxyl signals for four spin-labeled high-spin (h.s.) Fe(III) porphyrins showed partially resolved splittings at temperatures near 4 K. Axial ligands were fluoride, chloride, or bromide. As temperature was increased to 20 to 30 K the iron–nitroxyl splitting collapsed due to increasing rates of iron relaxation. Electron spin-echo (ESE) spectroscopy showed that above about 6 K collapse of the iron–nitroxyl spin–spin splitting caused a dramatic increase in the nitroxyl phase memory relaxation rates. Electron spin relaxation rates were determined for Fe(tetratolylporphyrin)X, X = F, Cl, Br, in toluene solution by ESE or inversion recovery at 4.5 to 6 K and by analysis of the temperature-dependent contributions to the continuous wave EPR linewidths between about 10 and 120 K. Above about 10 K iron relaxation rates increase in the order X = F < Cl < Br, which is the order of increasing zero-field splitting. Saturation recovery data for two spin-labeled h.s. iron(III) porphyrins between about 15 and 120 K and for two additional spin-labeled h.s. iron(III) porphyrins between about 85 and 120 K demonstrated that interaction with the h.s. iron enhanced the electron spin relaxation rate of the spin label. The saturation recovery curves for the nitroxyl were analyzed to determine interspin distances using a modified version of the Bloembergen equation and independently determined iron relaxation rates. Interspin distances were between 11.6 and 15.0 Å, were independent of axial ligand, and were in good agreement with values obtained previously for low-spin Fe(III) and Cu(II) analogs.

INTRODUCTION

There is a significant number of proteins that contain, in accessible oxidation states, two native paramagnetic centers (*1, 2*). This list includes a growing number of metalloenzymes that involve interaction between two inequivalent paramagnetic centers, including, for example, Co(II) with organic radicals in B_{12}-dependent enzymes (*1*), iron–sulfur cluster with the Ni–C center in nickel-containing hydrogenase (*2, 3*), iron oxo-dimer with tyrosyl radical in ribonucleotide reductase (*1*), and heme with flavin radical in nitric oxide synthase and NADPH cytochrome P450 reductase (*4*). In these types of systems determination of the distance between the two paramagnetic centers provides a crucial clue to the spatial layout of the interacting partners.

Continuous wave (CW) electron paramagnetic resonance (EPR) has been used to obtain electron–electron interspin distances primarily via analysis of lineshape changes due to spin–spin splitting (*5*) or by measurement of the relative intensity of the half-field transition (*6*). The intensity of the half-field transition falls off as r^{-6} so it is useful primarily for relatively short interspin distances. Dipolar splittings have an r^{-3} dependence. The longest distances for which resolved lineshape changes can be observed depends upon linewidths, but 12–15 Å is a generous upper limit, except for systems with very narrow lines. To observe resolved spin–spin splittings the relaxation rate of both spins must be slow relative to the splitting, which limits the application of these methods to slowly relaxing metals. Electron spin relaxation times are expected to be sensitive to interaction with a rapidly relaxing spin over longer distances than can be detected by changes in CW lineshapes.

Impact of spin–spin interaction on nitroxyl T_1. Equation [1], which is based on the NMR work of Bloembergen and colleagues (*7–9*), and is sometimes referred to as the Bloembergen equation, describes the effect of a rapidly relaxing electron spin on the relaxation rate for a more slowly relaxing spin due to dipolar coupling in rigid media. It has been applied to mixtures of radicals with paramagnetic metal ions (*10, 11*) and to pairwise interaction between paramagnetic centers (*3, 4, 10, 12–23*). One early study (*11*) made the assumption that $T_{1f} = T_{2f}$ and replaced T_{2f} in Eq. [1] by T_{1f}. That version of the equation was subsequently used in situations where T_{1f} may not have been equal to T_{2f} (*12, 13*). Initially CW power saturation was used to measure T_{1s} (*10, 12–14, 16, 17*). More detailed information can be obtained by examining the full shape of the saturation recovery (SR) curve for the slowly relaxing partner. The dipolar interaction is anisotropic. In addition, for most metals, there is anisotropy in ω_f due to g anisotropy, A anisotropy, or zero-field splitting which causes significant anisotropy in $\omega_f - \omega_s$. In some cases there is anisotropy in T_{1f} and/or T_{2f}. The net effect of these anisotropies is that T_{1s} is different for different orientations of the molecule with respect to the external magnetic field. The resulting saturation curve is a

1090-7807/98 $25.00

superposition of responses from different orientations and is not a single exponential decay (*4, 18–23*). Simplified forms of Eq. [1] assume that the dipolar interaction is the only source of anisotropy in T_{1s} (*3, 4, 18–21*), which is not valid for metal ions with anisotropy, including the anisotropy for $S > 1/2$ with substantial zero-field splitting (ZFS).

$$\frac{1}{T_{1s}} = \frac{1}{T_{1s}^0} + S(S+1) \times \left[\underbrace{\frac{b^2 T_{2f}}{1 + (\omega_f - \omega_s)^2 T_{2f}^2}}_{B \text{ term}} + \underbrace{\frac{c^2 T_{1f}}{1 + \omega_s^2 T_{1f}^2}}_{C \text{ term}} + \underbrace{\frac{e^2 T_{2f}}{1 + (\omega_f + \omega_s)^2 T_{2f}^2}}_{E \text{ term}} \right] \quad [1]$$

$$b^2 = \frac{1}{6} g_s^2 g_f^2 \beta^4 \frac{(1 - 3\cos^2\theta)^2}{\hbar^2 r^6}$$

$$c^2 = 3 g_s^2 g_f^2 \beta^4 \frac{\sin^2\theta \cos^2\theta}{\hbar^2 r^6}$$

$$e^2 = \frac{3}{2} g_s^2 g_f^2 \beta^4 \frac{\sin^4\theta}{\hbar^2 r^6},$$

where ''f'' and ''s'' denote the fast and slowly relaxing spins, respectively; T_{1s}^0 is T_1 for the slowly relaxing spin in the absence of spin–spin interaction; T_{1s} is T_1 for the slowly relaxing spin perturbed by the fast relaxing spin; S is the electron spin on the faster relaxing center; ω_f and ω_s are the resonant frequencies for the fast and slowly relaxing spins, respectively; r is the interspin distance; and θ is the angle between the interspin vector and the external magnetic field.

Equation [1] includes only the dipolar contribution to the spin–spin interaction. Exchange interaction also can contribute to enhanced relaxation of the slowly relaxing partner. In some reports the exchange contribution was added to Eq. [1] as a separate term in J^2 (*3, 4, 18–21*). However, the exchange interaction contributes to the same $S_{1\pm}S_{2\mp}$ matrix elements of the spin–spin interaction Hamiltonian that are the basis for the B term in Eq. [1]. Since, in general, the sum of the squares is not equal to the square of the sum, the exchange contribution should be included by modifying b^2 as shown in the following equation (*22, 23*) rather than having a separate term involving J^2.

$$b^2 = \frac{8}{3}\left[-\frac{J}{2} - \frac{1}{4} g_s g_f \beta^2 \frac{(1 - 3\cos^2\theta)}{\hbar r^3} \right]^2, \quad [2]$$

where J in units of s^{-1} is the electron–electron exchange interaction for the Hamiltonian written as $-JS_1 \cdot S_2$.

For systems in which the EPR spectra of the rapidly and slowly relaxing spins overlap, the factor of $\omega_f - \omega_s$ in the denominator of the B term can become very small for some orientations of the molecule. To ensure that T_{1s} approaches T_{1f} in the limit as $\omega_f - \omega_s$ becomes small, we proposed modification of the B term (*22, 23*) as

$$\text{Modified } B \text{ term:} \quad \frac{b^2 T_{2f}}{1 + (\omega_f - \omega_s)^2 T_{2f}^2 + b^2 T_{1f} T_{2f}}. \quad [3]$$

Equation [1] is the rigid-lattice version of the Solomon equation that is widely used to interpret NMR spectra of paramagnetic molecules in fluid solution (*24*). To obtain the Solomon equation from Eq. [1] the angular-dependent terms are replaced by spherical averages because it is assumed that tumbling is fast enough to average the orientation dependence of the dipolar interaction.

The factor of $S(S + 1)$ in Eq. [1] and in the Solomon equation relies on the assumption that the Curie law is obeyed (*25*). For $S > 1/2$ this will be valid at temperatures where kT is significantly greater than the ZFS. In NMR studies it has been observed that proton relaxation enhancement for metals with large ZFS is not as large as predicted by the Solomon equation (*24*). We have also observed that the impact on nitroxyl relaxation of h.s. Fe(III) porphyrins ($S = 5/2$) is not as much greater than for low-spin (l.s.) Fe(III) porphyrins ($S = 1/2$) as expected for the differences in magnetic moment (*26*). For a metal with $S = 5/2$ and ZFS greater than the EPR quantum, the $m_s = \pm 1/2$ transition has ω_f approximately equal to the EPR quantum, but other transitions have ω_f of the order of 2D and 4D. The large values of ω_f for these transitions result in such large denominators for the B and E terms in Eq. [1] that these other transitions do not contribute effectively to enhanced relaxation. To take account of the ineffectiveness of these transitions in enhancing the relaxation of the slowly relaxing spin we propose, as a first approximation, to add a weighting factor to the B and E terms. The weighting factor is the fraction of fast relaxing spins with $m_s = \pm 1/2$ at a particular temperature and zero-field splitting calculated from the Boltzmann populations of the three Kramers' doublets. It is assumed that other transitions make such a small contribution to the B and E terms that to first approximation they can be neglected. A similar factor does not apply to the C term because the denominator depends only on ω_s and not on ω_f.

Impact of spin–spin interaction on nitroxyl T_m. In rigid media the iron–nitroxyl interaction also impacts the nitroxyl T_m. In mixtures of organic radicals with more rapidly relaxing centers the impact of spin–spin interaction on ESE decay curves has been analyzed to determine the spatial distributions of the paramagnetic centers (*27*). For pairwise interaction between inequivalent paramagnetic centers the dominant effect on T_m for the slowly relaxing center is analogous to the effects of a dynamic physical process that aver-

ages inequivalent nuclei to which the unpaired electron is spin-coupled (*22, 23*). As temperature is increased and the relaxation rate of the more rapidly relaxing center becomes comparable with the splitting of the EPR signal due to spin–spin interaction there is an uncertainty in the resonance frequency and a decrease in T_m for the slowly relaxing center. Further increase in the relaxation rate of the faster relaxing center gives an averaged signal and an increase in T_m for the slowly relaxing center. Equations for analyzing the effect of a two-site averaging process on the ESE decay were derived by Zhidomirov and Salikhov (*28*) and have been used to analyze the effects of rotation of methyl groups in acetate anion (*29*) and in nitroxyl radicals (*30*). When these equations were used to analyze the decays for spin-labeled l.s. Fe(III) complexes as a function of temperature it was observed that the effective correlation time was $\sqrt{T_{1f}T_{2f}}$ (*22, 23*). The involvement of both T_{1f} and T_{2f} reflects the fact that either a T_1 flip or a T_2 flip for the rapidly relaxing center causes a change in the resonant frequency of the slowly relaxing center to which it is spin-coupled and thereby constitutes a dephasing mechanism.

To examine the effects of high-spin Fe(III) on nitroxyl relaxation SR and ESE data were obtained for high-spin Fe(III) complexes of the spin-labeled porphyrins shown below. The axial ligands were fluoride, chloride, and bromide, which span a range of values of ZFS. These spin-labeled porphyrins were selected for the initial study of h.s. Fe(III) to permit comparison with previous determinations of interspin distances for the low-spin Fe(III) analogs by time-domain EPR (*22*) and for Cu(II) analogs by CW EPR of doped single crystals (*31*).

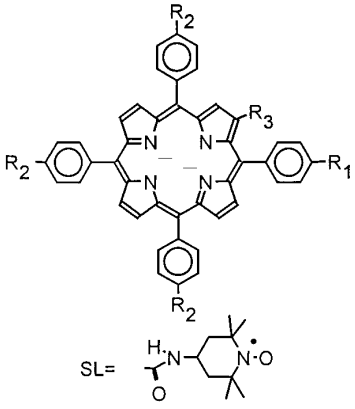

R_1	R_2	R_3	
SL	CH_3	H	*p*-TTP-SL
H	H	*cis* -CH=CH-SL	*cis*-TPP-SL
H	H	*trans* -CH=CH-SL	*trans*-TPP-SL
H	H	*trans* -CH=CH-COOEt	*trans*-TPP-ester
H	H	$-CH_2-CH_2$-SL	*satd*-TPP-SL
H	H	H	TPP
CH_3	CH_3	H	TTP

EXPERIMENTAL

Preparation of compounds. Fe(TPP)Cl (*22*), Fe(TTP)Cl (*22*), Fe(*cis*-TPP-SL)Cl (*22*), Fe(*trans*-TPP-SL)Cl (*22*), Fe(*sat'd*-TPP-SL)Cl (*22*), $[Fe(p\text{-TTP-SL})]_2O$ (*22, 32*), Fe(*trans*-TPP-ester)Cl (*33*), H_2(*trans*-TPP-SL) (*33*), and H_2(*p*-TTP-SL) (*33*) were prepared by literature methods. Products were characterized by visible and EPR spectroscopy (*22, 33*).

Preparation of solutions for EPR studies. The solid (isolated) samples of the iron porphyrin chlorides typically contained some oxo-bridged dimer. To ensure that all of the iron existed as the 5-coordinate monomer, each complex was treated with base to form the 5-coordinate hydroxide which spontaneously converts to the oxo-bridged dimer. Then the dimer was treated with a dilute aqueous acid solution to make the 5-coordinate halide. In preparing samples from isolated solids that were predominantly oxo-dimer, samples were shaken with base to ensure that all of the porphyrin was in the oxo-dimer form before being shaken with acid. The organic and aqueous phases were mixed by shaking by hand as reported previously (*22*) or by shaking with a WigLBug (Crescent Dental Co.) as described below. Compared to shaking samples by hand, the use of the WigLBug gave essentially complete and reproducible conversion of axial ligand while reducing the contact time of the organic solution with the acid solution from several minutes to 0.5 to 1.0 min and reducing the acid concentration from 2 to 1%. Samples were prepared and studied in toluene instead of the 2:1 toluene:chloroform mixture that was used to study the low-spin analogs (*22*) because residual HCl present even in carefully purified chloroform made it difficult to avoid contamination with axial chloride complexes.

In a 2.0-mL plastic microfuge tube 1.0 mL of 0.05 M aqueous NaOH was added to 1.0 mL of 1.0 mM iron(III)-porphyrin chloride in toluene. The tube was taped to the plate of the WigLBug where it was shaken for 2 min. The green toluene layer was removed with a glass pipet and transferred to a clean tube and the procedure was repeated.

After the second shaking with base, the toluene layer was again transferred to a clean tube, 1.0 mL of 1% aqueous H*X* (*X* = F, Cl, Br) was added, and the mixture was shaken with the WigLBug. Times for shaking were 0.5 min for HCl and 1.0 min for HBr or HF. After the shaking, the toluene solution was transferred to a clean, dry tube. In each transfer care was taken to separate the toluene solution from the aqueous layer. An aliquot of the final solution was transferred to a 4-mm EPR tube. The remainder of the solution could be stored in a glass container for up to 2 weeks at 0°C without degradation. Samples for relaxation time measurements were degassed by a minimum of three freeze–pump–thaw cycles, and then the tube was back-filled with a partial pressure of helium.

Below about 10 K the EPR spectra of FeTTPF and FeTTPBr in glassy solution exhibit characteristic splitting of the $g' = 2$ signal due to coupling to the nuclear spin of the F ($I = 1/2$, doublet) or Br ($I = 3/2$, quartet). The $g' = 2$ signal for FeTTPCl is a singlet. Complete conversion of axial ligand was indicated by the absence, within experimental uncertainty, of the singlet for FeTTPCl superimposed on the characteristic doublet (F) or quartet (Br) in the EPR spectra at liquid helium temperatures. Visible spectra as a function of axial ligand for FeTTPX in toluene were as follows with λ_{max} in nanometers and log(ϵ) in parentheses: *X* = F, 417 (5.19), 597 (3.78), 636 (3.73); *X* = Cl, 372 (4.76), 421 (5.10), 508 (4.17), 571 (3.61), 690 (3.61); *X* = Br, 388 (4.88), 422 (5.03), 512 (4.21), 576 (3.58), 699 (3.57).

Continuous wave EPR spectra. Spectra were obtained in the CW mode on locally constructed spin-echo (*34*) or saturation recovery (*35*) spectrometers with Varian TE_{102} resonators and an Oxford ER900 flow cryostat or on a Bruker ESP 380E with a split-ring resonator and Oxford ER935 cryostat. Temperatures for each system were calibrated by replacing the sample-containing tube with a tube containing a thermocouple immersed in 1:1 water:glycerol or a Lakeshore TG-120PL GaAl As diode immersed in silicone oil. Temperatures were measured with a Lakeshore readout that was calibrated with liquid nitrogen and liquid helium. The uncertainty in temperature is estimated to be ±1 K.

Saturation recovery measurements. A locally constructed spectrometer (*35*) operating at 9.2 GHz was used for the SR measurements. Temperatures between 5 and 70 K were obtained with liquid helium and an Oxford ER900 flow cryostat. Temperatures between 80 and 120 K were obtained with liquid nitrogen and a Varian Dewar flow assembly. To test for spectral diffusion the pump time was increased until further increase gave no detectable change in the recovery time constant. Pump times used for data collection were $>T_1$. Typically 5000 to 10,000 recovery curves were signal averaged in a LeCroy digital oscilloscope or with an EGG 9825 digitizer and stored in a PC. SR data for the spin-labeled high-spin Fe(III) porphyrins were recorded in the center of the nitroxyl spectrum at temperatures between about 10 and 120 K. The dependence of the SR data on position in the spectrum was examined at 100 K.

Electron spin-echo measurements. Two-pulse spin-echo experiments were performed either on a locally constructed spectrometer (*34*) operating at ca. 9.2 GHz with an overcoupled Varian V4531 TE_{102} resonator and an Oxford ER900 flow cryostat or on a Bruker ESP380E with a split-ring resonator and an Oxford ER935 cryostat. Data for the iron signals were recorded on the ESP380E using 16- and 24-ns pulses and incident power selected for maximum echo intensity. On the locally constructed system nitroxyl data were collected with 20- and 40-ns pulses and a dead time of 200 ns. On the ESP380E pulse widths for the nitroxyl samples were 40 and 80 ns and the dead time was about 100 ns. Typically, echo decays of 256 to 512 data points were recorded extending for 2 to 15 μs. On the locally constructed spectrometer the boxcar aperture was set to encompass the full width at half-height of the echo. On the ESP380E an integrator module was used to digitize the echo.

The time constant for the ESE decay is referred to as T_m to encompass all processes that result in echo dephasing, including the collapse of iron–nitroxyl splitting by the iron electron spin relaxation. The values obtained directly from experiment are typically cited as decay time constants. In the ensuing discussion it is often more direct to refer to relaxation rates, which are the reciprocals of the time constants. For 1 mM glassy solutions of nitroxyl radicals at the temperatures and pulse lengths examined in these studies, T_m is weakly dependent upon pulse turning angle, which indicates that instantaneous diffusion (*36*) makes only a minor contribution to T_m. To the extent that this process contributes to T_m, it will be about the same for H_2(*trans*-TPP-SL), for H_2(*p*-TTP-SL) and for the spin-labeled iron complexes and does not contribute to differences between them.

To determine the temperature dependence of echo intensity for Fe(*p*-TTP-SL)*X* the echo amplitude at 100 ns was measured on a LeCroy 9410 oscilloscope at a repetition time that was long relative to the nitroxyl T_1. For samples of Fe(*trans*-TPP-SL)*X*, Fe(*cis*-TPP-SL)*X*, and Fe(*sat'd*-TPP-SL)*X* the echo amplitude at long repetition time, I_∞, was estimated using the relationship $I_t = I_\infty[1 - e^{-t/T_1}]$, where *t* is the pulse repetition time.

Direct measurements of T_1 and T_2 for high-spin Fe(III) by inversion recovery or ESE, respectively, were performed at 4.5 to 6 K and the data were fitted to a single exponential. Inversion recovery measurements were performed on the ESP380E with a $\pi-T-\pi/2-\tau-\pi-\tau-$echo sequence. For FeTTP*X*, and for the iron signals in the spin-labeled complexes, the value of T_m was independent of pulse turning

angle which indicates that instantaneous diffusion (*36*) makes a negligible contribution to the dephasing process. The high-spin Fe(III) EPR signal extends over about 2300 G so the probability that a neighboring Fe(III) is flipped by the second microwave pulse and thereby changes the resonance of the observed iron is negligibly small. There were no indications of processes other than T_2 that might contribute to T_m for the iron so T_m was assumed to be a reasonable estimate of T_2.

ANALYSIS OF EXPERIMENTAL DATA

Analysis of CW spectra of high-spin Fe(III) to determine T_2. The powder spectra of the high-spin Fe(III) complexes were simulated with a locally written program (SATMON) in which the lineshape is a Gaussian distribution of Lorentzian spin packets characterized by T_2. Simulations were based on fictitious $S = 1/2$ and the effective g values obtained by the simulations are denoted as g'. The widths of the Gaussian distributions and the values of T_2 can be orientation dependent. At low temperature the orientation-dependent T_2 values were defined by the ESE experiments and the g' values, hyperfine splittings, and widths of the Gaussian distribution were adjusted to fit the spectra. Hyperfine splitting and the widths of the Gaussian distributions were assumed to be independent of temperature. The temperature-dependent contribution to the linewidths at temperatures above about 10 K were simulated by varying the value of T_2.

The g' values for the $m_s = \pm 1/2$ transitions of the high-spin Fe(III) were approximately 6.0 and 2.0 for all of the complexes, within the uncertainty in field-sweep calibration. For FeTTP*X* and Fe(*trans*-TPP-ester)*X* g' anisotropy in the x,y plane ($|g'_x - g'_y|$) increased in the order X = Br (0.0) < Cl (0.02) < F (0.2). Resolved hyperfine splittings along g'_z were $A_z^{Br} = 0.00205$ cm^{-1} for Fe(*trans*-TPP-ester)Br, FeTPPBr, and FeTTPBr and $A_z^F = 0.0041$ cm^{-1} for Fe(*trans*-TPP-ester)F and FeTTPF. These hyperfine splittings are comparable to values reported in the literature: $A_z^{Br} = 0.00261$ cm^{-1} for Fe(deuteroporphyrin dimethylester)Br in THF-chloroform (*37*) and 0.00256 cm^{-1} for Fe(protoporphyrin dimethylester)Br in THF-chloroform (*37*); $A_z^F = 0.0042$ cm^{-1} for FeTPPF in solid H_2TPP (*38*) and 0.0044 cm^{-1} for Fe(protoporphyrin dimethylester)F or Fe(deuteroporphyrin dimethylester)F in THF-chloroform (*37*). Hyperfine splitting was not resolved along $g' \sim 6$. Hyperfine splittings in the perpendicular plane were adjusted along with the width of the Gaussian distribution to fit the observed low-temperature linewidths. The values of $A_\perp$ that were used in the simulations were 28×10^{-4} cm^{-1} for X = Br and 40×10^{-4} cm^{-1} for X = F. The widths (w_i) of the Gaussian distributions that were used in the simulation for FeTTP*X* were X = Br; $w_x = w_y = 20$ G, $w_z = 7$ G; X = Cl; $w_x = 9$, $w_y = 40$, $w_z = 7$ G; X = F; $w_x = w_y = 25$, $w_z = 8$ G. Similar widths of the distributions were used for the unsymmetrically substituted porphyrins, including the spin-labeled porphyrins.

Simulation of nitroxyl spectrum at 100 K. CW spectra of H_2(*trans*-TPP-SL) and H_2(*p*-TTP-SL) at 100 K were analyzed using the locally written program MONMER, which is based on perturbation calculations, assumes that the principal axes of the **g** and **A** matrices are collinear, and treats hyperfine interactions to second order (*39*). Nitroxyl parameters were $g_x = 2.0095$, $g_y = 2.0053$, and $g_z = 2.0025$; $A_x = 4 \times 10^{-4}$, $A_y = 6 \times 10^{-4}$, and $A_z = 33.5 \times 10^{-4}$ cm^{-1}.

Analysis of saturation recovery data for spin-labeled complexes. The nitroxyl SR data were simulated using Eqs. [1]–[3] and the weighting factor for the B and E terms described in the Introduction. A random distribution of molecular orientations with respect to the external magnetic field was included. For each molecule there is a defined angle, ϵ, between the interspin vector and the z axis of the Fe(III) ZFS tensor. Since the rhombic distortion of g' is very small, a second angle is not needed to define the orientation. Since the true g values for the high-spin Fe(III) are approximately isotropic and the anisotropy of the g values for the nitroxyl is very small, there is insignificant anisotropy of g_s and g_f in the calculation of the dipolar interaction and the anisotropy of the dipolar splitting is determined by the dependence on θ in Eq. [1]. For each orientation of the molecule $\omega_f - \omega_s$ was calculated using the principal components of g', ϵ, and the orientation of the interspin vector relative to the external magnetic field. The anisotropy of $\omega_f - \omega_s$ is a major contribution to the anisotropy of T_{1s}. Since the dipolar interaction falls off as r^{-6} and the average intermolecular distance in a 1 mM solution, for a random distribution (*40*), is about 66 Å, it was assumed that the intramolecular iron–nitroxyl interaction (r = 10 to 15 Å, see below) dominated and that intermolecular interaction could be neglected. The nitroxyl T_{1s} at each orientation was calculated and the contributions to the SR curve were summed using the appropriate solid angle weighting, analogous to what is done in simulating CW powder spectra.

If one could obtain orientation-selective relaxation time information it could be used to separate exchange and dipolar contributions to the spin–spin interaction. However, in the spin-labeled complexes the nitroxyl T_1 showed little variation with position in the EPR spectrum at 100 K. At X band, possibilities for orientation selection based upon position in the nitroxyl spectrum are limited by the orientation dependence of the nitroxyl nitrogen hyperfine splitting (about 30 G). The selectivity is decreased by unresolved proton hyperfine splitting which contributes about 7 G to the linewidths in glassy solution. The interspin distances observed for these complexes (10–15 Å) result in maximum dipolar splittings

that are of the same order of magnitude as the nitroxyl hyperfine splitting, which obscures orientation selection at these interspin distances. The interspin distances were calculated from data obtained in the middle of the nitroxyl spectrum where there is maximum overlap of transitions from multiple orientations. Orientation selection was not included in the calculations because it was judged to have less impact than experimental error.

Input parameters for analysis of nitroxyl SR data. The values of T_{1s}^{0} were obtained from SR measurements on H_2(*trans*-TPP-SL) or H_2(*p*-TTP-SL). Values of T_{2f} at temperatures above about 10 K were obtained by analysis of the temperature-dependent contributions to the iron CW lineshapes as discussed above. Between 4 and 6 K the temperature dependence of T_{1f} is greater than for T_{2f} and the data suggest $T_{1f} \sim T_{2f}$ above about 10 K. The values of ϵ, the angle between the interspin vector and the ZFS axes of the Fe(III), that were used in the simulations were based on the known geometries of the complexes and the values observed in the single-crystal EPR studies of Cu(*trans*-TPP-SL) and Cu(*cis*-TPP-SL) (*31*): Fe(*sat'd*-TPP-SL)*X*, ϵ = 45°; Fe(*cis*-TPP-SL)*X*, ϵ = 60°; Fe(*trans*-TPP-SL)*X*, ϵ = 90°; Fe(*p*-TPP-SL)*X*, ϵ = 90°. The simulated SR curves were weakly dependent on the value of ϵ. Values of the ZFS splitting parameter *D* for FeTPPCl determined by a variety of techniques are between 6.0 and 8.0 cm^{-1} (*41–45*) so 7.0 cm^{-1} was taken as an average. For FeTPPBr, $D = 12.5\ cm^{-1}$ (*46*). For FePX, *D* increases in the order F < Cl < Br (*47*) and typically is smaller for FeTTP*X* than for Fe(protoporphyrin IX dimethyl ester)*X*. Since the value of *D* for Fe(protoporphyrin IX dimethyl ester)F is 5.0 cm^{-1} (*47*), the value of *D* for FeTTPF was estimated as 4 cm^{-1}. The simulated SR curves at temperatures above 15 K were insensitive to changes of $\pm 1\ cm^{-1}$ in the value of *D*. The remaining unknowns in Eqs. [1]–[3] are *r* and *J*. The value of *r* was adjusted to give the best fit to the experimental data with $J = 0$. The use of nonzero values of *J* did not improve the fit to the data. As discussed below, the CW spectra indicate that the value of *J* in these complexes is significantly less than the *z* component of the nitroxyl nitrogen hyperfine splitting, i.e. $J \ll 35$ G. To estimate the magnitude of the error in *r* that could occur due to neglect of exchange interaction of this magnitude, simulations of the SR data for Fe(*trans*-TPP-SL)*X* were performed with $|J| = 5$ G. The resulting values of *r* were longer by about 0.5 Å than when exchange was not included. Thus for interspin distance of the magnitude observed in this study, neglect of an exchange interaction of the order of 5 G is not a major source of error.

Analysis of spin-echo data for nitroxyl in spin-labeled complexes. The analysis of the spin-echo data was the same as that used for the low-spin analogs (*22, 28*) except that the factor of $\frac{3}{4}$ used in the calculation of dipolar splitting for $S = 1/2$ was replaced by the more general $S(S + 1)$. Although the collapse of splitting due to interaction with the high-spin Fe(III) is more complicated than a two-site exchange, the approximation as two-site is comparable to the approximation of methyl group rotation as a two-site exchange. Only orientations of the nitroxyl that result in resonance within ±3 to 5 G of the center of the nitroxyl spectrum were included in the calculation (*22*). Parameters for the analysis of the ESE data for Fe(*p*-TTP-SL)*X* were the same as in the analysis of the SR data. As in the analysis of the SR data it was assumed that intermolecular iron–nitroxyl interaction could be neglected.

The values of T_{1f} and T_{2f} between 5 and 10 K were interpolated between the values obtained by ESE and inversion recovery below 6 K and the values obtained by analysis of the iron CW lineshapes above 10 K. In the slow averaging limit (Eq. [5] of Ref. *22*), the effect of the iron on the nitroxyl T_m is independent of the splitting that is collapsed and depends only on the rate of the dynamic process. For spin-labeled low-spin Fe(III) porphyrins the observed temperature dependence of the dynamic process was that of $\sqrt{T_{1f}T_{2f}}$ (*22*). A similar dependence was observed for the high-spin complexes reported here.

RESULTS

CW spectra of high-spin Fe(III). The CW spectra of FeTTP*X*, *X* = F, Cl, Br, exhibited characteristic turning points at $g' \sim 6$ and $g' \sim 2$ due to the $m_s = \pm 1/2$ transitions. Near 4 K the linewidths were independent of temperature and are attributed to a distribution in g' values and unresolved hyperfine splitting, which is assumed to be independent of temperature. The temperature-dependent contribution to the linewidths at higher temperatures is attributed to increasing rates of electron spin relaxation with increasing temperature. The low-temperature linewidths for the $g' \sim 2$ signals were narrower (7–10 G, depending on axial ligand) than the linewidths for the $g' \sim 6$ signals (20–40 G). In addition, the conversion between $1/T_2$ in s^{-1} and linewidth in gauss depends inversely on the g' value. Because of these two factors the contribution to the linewidth from electron spin relaxation was observable above 8 (*X* = Br) to 10 K (*X* = F) for the $g' \sim 2$ turning point whereas significant changes in the $g' \sim 6$ linewidth were observable only above 15 (*X* = Br) to 20 K (*X* = F). Due to the lower populations at the $g' \sim 2$ turning point, the $g' \sim 2$ signal became indistinguishable from background at a lower temperature than did the $g' \sim 6$ signal, so the width of the $g' \sim 6$ signal could be measured at higher temperatures than the width of the $g' \sim 2$ signal.

The values of T_2 for FeTTP*X*, *X* = F, Cl, Br, determined by simulation of the CW spectra of the $m_s = \pm 1/2$ transitions are shown in Fig. 1. In the temperature range in which electron spin relaxation made an observable contribution to the CW lineshapes the values of T_2 along $g' \sim 2$ and $g' \sim 6$

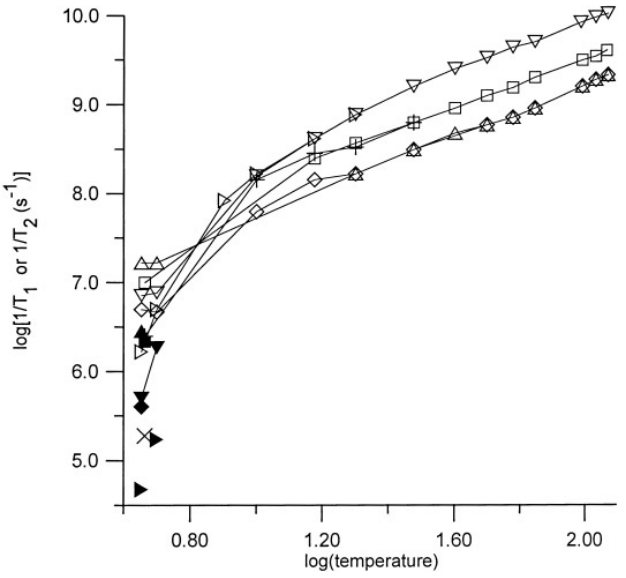

FIG. 1. Electron spin relaxation rates for Fe(III) $m_s = \pm 1/2$ transitions of FeTTPX in toluene as a function of temperature. Values of T_2 between 4 and 6 K were obtained by ESE and values at higher temperature were obtained by simulation of the temperature-dependent contributions to the CW lineshape. Values of T_1 between 4 and 6 K were measured by inversion recovery. (△) X = F, $T_{2\perp}$; (◇) X = F, $T_{2\|}$; (▲) X = F, $T_{1\perp}$; (◆), X = F, $T_{1\|}$; (□) X = Cl, $T_{2\perp}$; (+), X = Cl, $T_{2\|}$; (■) X = Cl, $T_{1\perp}$; (×) X = Cl, $T_{1\|}$; (▽), X = Br, $T_{2\perp}$; (▷) X = Br, $T_{2\|}$; (▼) X = Br, $T_{1\perp}$; (▶) X = Br, $T_{1\|}$. The lines on the graphs connect the data points.

were the same within experimental uncertainty. In the spin-labeled complexes the nitroxyl signal obscured the $g' \sim 2$ turning point for the Fe(III). However, for each axial ligand, iron T_2 values calculated from the $g' \sim 6$ Fe(III) signals as a function of temperature for Fe(p-TTP-SL)X were the same, within experimental uncertainty, as the values obtained for FeTTPX. The values of T_2 determined from the CW lineshapes for Fe(*trans*-TPP-ester)Br and Fe(TPP)Br were within experimental uncertainty of the values for Fe(TTP)Br. Thus, for these complexes, the substituents on the phenyl or pyrrole rings do not appear to have significant effects on the rate of iron electron spin relaxation. The values of T_2 for Fe(TTP)X (Fig. 1) were used in the analysis of the SR and ESE data for the spin-labeled complexes with the same axial ligand.

Time-domain measurements of iron(III) relaxation times. At 4 to 6 K T_m and T_1 for the iron signal were measured by ESE and inversion recovery, respectively. It was assumed that $T_m \sim T_2$. In this temperature interval the relaxation times decreased monotonically as g' increased from 2 to 6 and T_1 was significantly longer than T_2 (Fig. 1). For example, for FeTTPCl in toluene at 4.5 K $T_{2\|} = 0.4$ μs, $T_{2\perp} = 0.1$ μs, $T_{1\|} = 5$ μs, and $T_{1\perp} = 0.5$ μs. For high-spin Fe(III) in methemoglobin and metmyoglobin at temperatures near 4 K power saturation studies and time-domain measurements indicated longer relaxation times along the parallel axis than in the perpendicular plane (*48–50*). The absence of a similar orientation dependence at higher temperatures suggests that the dominant relaxation mechanism changes with temperature.

Since the ZFS for the h.s. Fe(III) porphyrins is greater than the X-band EPR quantum, only transitions between the $m_s = \pm 1/2$ levels are observed. Electron spin relaxation times may be different for different values of m_s. Relaxation between $m_s = \pm 1/2$ and $m_s = \pm 3/2$ as well as relaxation between the $m_s = \pm 1/2$ levels contributes to the temperature-dependent linewidths and to the time-domain measurements for the $m_s = \pm 1/2$ transition. As discussed in the Introduction, for the B and E terms in Eqs. [1]–[3] we assume that the iron $m_s = \pm 1/2$ transitions are the only transitions that make significant contributions to the enhanced relaxation of the nitroxyl. Thus the approximation that the measured values are adequate estimates of the iron relaxation times for all values of m_s introduces uncertainty only for the C term.

CW nitroxyl spectra. At 6 to 8 K the nitroxyl regions of the CW spectra of the spin-labeled high-spin Fe(III) complexes exhibited partially resolved splittings due to iron–nitroxyl interaction (Figs. 2–4). In the absence of iron–nitroxyl interaction, the nitroxyl relaxation time at 6 to 8 K is so long that CW spectra at the lowest microwave powers and modulation frequencies available on commercial spectrometers are seriously distorted by passage effects. The decrease in relaxation time due to interaction with the Fe(III) makes it possible to obtain CW spectra of the nitroxyl in the spin-coupled complexes. Spectra were checked for passage effects.

In spin-labeled high-spin Fe(III) porphyrins with J that is large relative to $\omega_f - \omega_s$, EPR signals are observed at average g values (*51*). If J is less than $\omega_f - \omega_s$ but larger than the nitroxyl hyperfine splitting, large splittings of the iron and nitroxyl signals are observed at low temperature (*52*). Unlike those cases, the nitroxyl spectra in Figs. 2–4 are characteristic of much weaker iron–nitroxyl interaction. Scans wider than those shown in Figs. 2–4 indicated the absence of additional signals due to stronger spin–spin interaction. The spectra in Figs. 2C and 3C show partially resolved splittings of about 18 G on the high-field A_Z line, reduced relative intensity in the center of the spectrum, and a sharp component in the center. If an exchange interaction dominated, the splittings would be approximately isotropic, which is not the case for any of the samples examined in this study. The observed low-temperature spectra are characteristic of an interaction that is dominated by an anisotropic dipolar interaction. Although the spectra are not well enough resolved to determine the exchange and dipolar contributions, the value of J must be much smaller than the nitrogen hyperfine splitting. The smaller splittings in the low-temperature spectrum of Fe(p-TTP-SL)Br (Fig. 4C) than in the

spectrum of Fe(*trans*-TPP-SL)Br (Fig. 2C) indicate weaker electron–electron interaction for Fe(*p*-TTP-SL)Br than for Fe(*trans*-TPP-SL)Br. The apparently greater broadening for the high-field and low-field A_Z lines than in the center of the spectrum again indicates that there is a large anisotropic contribution to the electron–electron interaction for this sample.

As the temperature was increased the splittings of the nitroxyl spectra collapsed due to increasing rates of iron electron spin relaxation (Figs. 2–4). Above about 30 K the nitroxyl regions of the CW spectra of the spin-labeled iron(III) porphyrins were typical of immobilized spin label. Collapse of the iron–nitroxyl splitting occurs when $1/\sqrt{T_{1f}T_{2f}}$ in s^{-1} is of the same order of magnitude as the iron–nitroxyl spin–spin splitting expressed in s^{-1} (*22*). The collapse occurs at lower temperature when the axial ligand is Br^- (Fig. 2) than when it is F^- (Fig. 3) because at the same temperature the iron relaxation rate is faster in the complexes with axial bromide than with axial fluoride (Fig. 1).

In toluene solution at room temperature the CW spectra

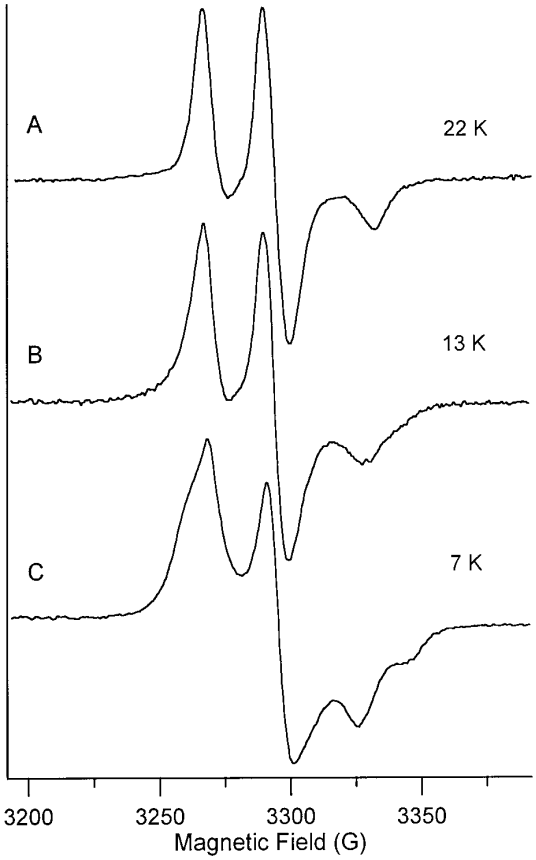

FIG. 2. CW spectra of Fe(*trans*-TPP-SL)Br in toluene at 9.24 GHz. Spectra were recorded in the CW mode of the SR spectrometer with 1 G modulation amplitude at 100 kHz and (A) 0.5 μW power at 22 K, (B) 0.15 μW power at 13 K, and (C) 0.15 μW power at 7 K.

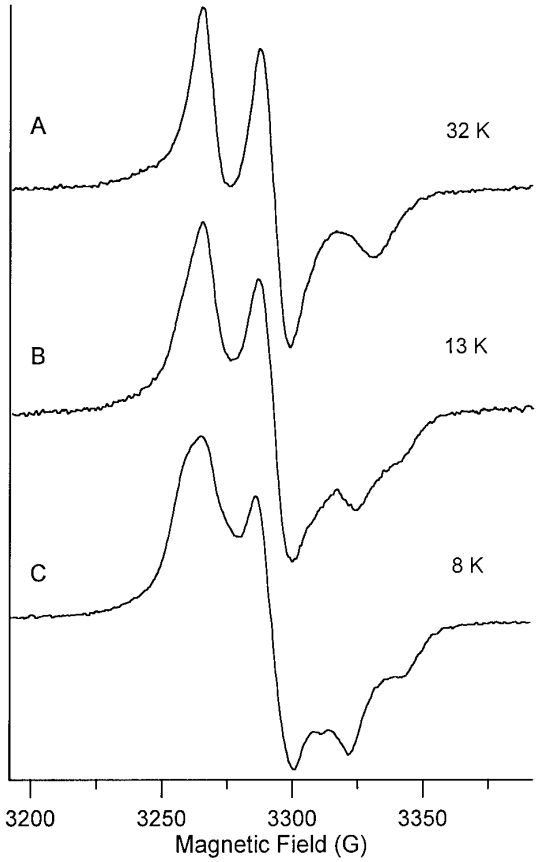

FIG. 3. CW spectra of Fe(*trans*-TPP-SL)F in toluene at 9.24 GHz. Spectra were recorded in the CW mode of the SR spectrometer with 1 G modulation amplitude at 100 kHz and (A) 4 μW power at 32 K, (B) 0.5 μW power at 13 K, and (C) 0.5 μW power at 8 K.

of the spin-labeled high-spin Fe(III) complexes exhibited a characteristic three-line nitroxyl signal. At this temperature the iron relaxation rate is so fast that there is no evidence in the unsaturated CW spectra of iron–nitroxyl interaction although power saturation curves show small effects of the Fe(III) on the nitroxyl relaxation rates (*53*). Except for two cases that are discussed below, double integration of 100-G CW spectra at room temperature or 200-G CW spectra at 100 K and comparison with integrals for standard samples of 4-oxo-2,2,6,6-tetramethylpiperidin-1-oxyl (4-oxo-tempo) obtained under comparable conditions showed that the intensity of the sharp characteristic nitroxyl signal accounted for all of the spin label in the sample.

In contrast, in a 0.4 mM toluene solution of Fe(*p*-TTP-SL)F at room temperature the integrated intensity of a 100-G scan corresponded to about 70% of that expected for the total nitroxyl in the sample. The fraction of the nitroxyl intensity observed in a 100-G scan decreased with increasing concentration of the solution (*32*). Since 100% of expected nitroxyl intensity was observed when the complex was present as [Fe(*p*-TTP-SL)]$_2$O, Fe(*p*-TTP-SL)Cl, or Fe(*p*-TTP-

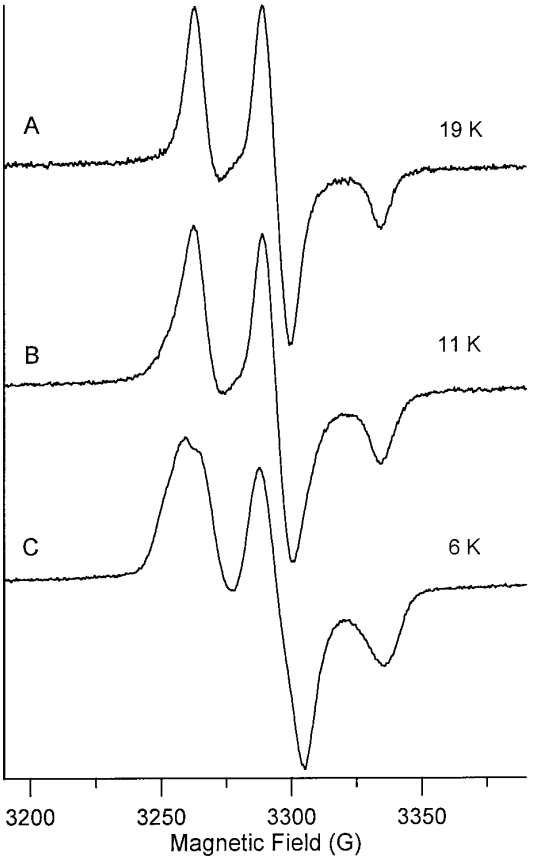

FIG. 4. CW spectra of Fe(p-TTP-SL)Br in toluene at 9.24 GHz. Spectra were recorded in the CW mode of the SR spectrometer with 1 G modulation amplitude at 100 kHz, 0.15 μW power and temperatures of (A) 19 K, (B) 11 K, and (C) 6 K.

SL)Br the low fraction of the nitroxyl intensity observed for Fe(p-TTP-SL)F is not due to incomplete spin labeling. Underlying the sharp nitroxyl signal in the spectra of Fe(p-TTP-SL)F there was a broad poorly defined component that is attributed to a species with stronger iron–nitroxyl interaction. When concentration was increased, the relative intensity of the broad component increased and the integrated intensity of the sharp signal decreased. It is proposed that there is an equilibrium with a dimeric species in which intermolecular interaction provides a pathway for stronger iron–nitroxyl interaction than the intramolecular pathway in the monomer (*32*). Addition of 5% by volume of the strong hydrogen-bonding agent 2,2,2-trifluoroethanol (CF_3CH_2OH) caused the integrated intensity of the sharp nitroxyl signal to return to 97% of the total nitroxyl present in the sample. Similarly, for a 1.2 mM solution of Fe(*sat'd*-TPP-SL)F the integrated intensity of a 200-G scan at 100 K was about 18% of that expected for the total nitroxyl concentration. Addition of 5% CF_3CH_2OH caused an increase in the integrated intensity to 44% of the expected value. These results suggest that the pathway for a stronger iron–nitroxyl interaction involves hydrogen bonding to the axial fluoride, which is possible for certain porphyrin–nitroxyl linkages. In reactions of FeTPPX, X = F, Cl, with imidazole it has been observed that hydrogen bonding to the axial ligand played a major role for X = F but not for X = Cl (*54*). This observation is consistent with our proposal that the difference in behavior of Fe(p-TPP-SL)X, X = F and Cl, is due to stronger hydrogen bonding with the axial F than with axial Cl. Due to the presence of more than one species in the solutions of Fe(p-TTP-SL)F and Fe(*sat'd*-TPP-SL)F, these samples were not included in the time-domain studies.

Electron spin–lattice relaxation for spin-labeled porphyrins. For H_2(*trans*-TPP-SL) between 25 and 120 K a plot of $\log(1/T_1)$ vs log(temperature) (Fig. 5) has a slope of 2.33 which is in the range observed for a wide variety of nitroxyl radicals in this temperature interval (*55*). For a 1.2 mM toluene solution of H_2(p-TTP-SL) in the same temperature interval the slope of an analogous plot was 2.21 (Fig. 6). However, below about 25 K the values of $\log(1/T_1)$ for the 1.2 mM solution of H_2(p-TTP-SL) decreased less rapidly than predicted by this line (Fig. 6) and the decays could not be fit with a single exponential. Aggregation is known to occur for porphyrins (*56*) and might contribute to increased rates of electron spin–lattice relaxation. To test for aggregation a toluene solution that contained 0.3 mM H_2(p-TTP-SL) and 1.0 mM H_2(p-TTP-NH_2) was examined. To the extent that aggregation occurs in this sample the nearest neighbor is more likely to be a diamagnetic porphyrin than a spin-labeled porphyrin. At 95 to 120 K the values of T_1

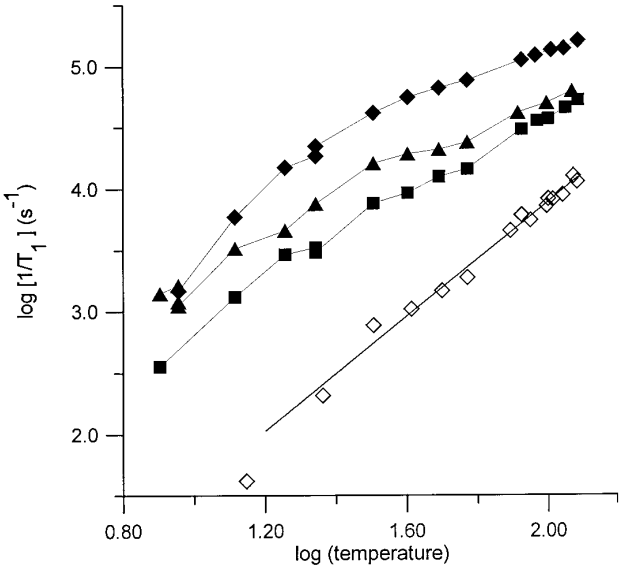

FIG. 5. Nitroxyl relaxation rates as a function of temperature in toluene solution for (◇) H_2(*trans*-TPP-SL); the least-squares fit line is $\log(1/T_1) = 2.33 \log(T) - 0.76$.; (■), Fe(*trans*-TPP-SL)F; (▲) Fe(*trans*-TPP-SL)Cl; (◆) Fe(*trans*-TPP-SL)Br. The lines through the data for Fe(*trans*-TPP-SL)X connect the data points.

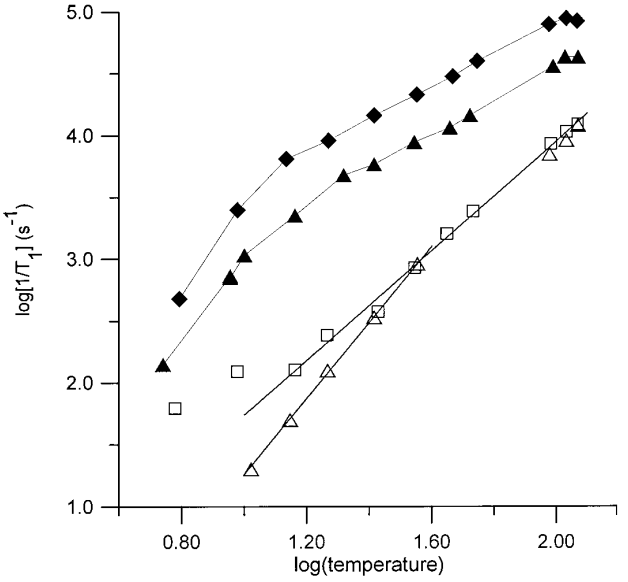

FIG. 6. Nitroxyl relaxation rates as a function of temperature in toluene solution for (□) 1.2 mM H_2(*p*-TTP-SL); the least-squares fit line is $\log(1/T_1) = 2.21 \log(T) - 0.47$; (△) 0.3 mM H_2(*p*-TTP-SL) + 1.0 mM H_2(*p*-TTP-NH_2); the least-squares fit to data below 30 K is $\log(1/T_1) = 3.06 \log(T) - 1.8$; (▲) Fe(*p*-TTP-SL)Cl; (♦) Fe(*p*-TTP-SL)Br. The lines through the data for Fe(*p*-TTP-SL)*X* connect the data points.

for the nitroxyl in the mixed porphyrin sample differed by less than 20% from values obtained for 1.2 mM H_2(*p*-TTP-SL), which is consistent with prior observations that T_1 values for 0.1 to 1 mM solutions of nitroxyl radicals at temperatures in the vicinity of 100 K are not strongly concentration dependent (*55*). Below about 20 K the values of T_1 obtained for the nitroxyl in the mixed porphyrin sample were significantly longer than those for H_2(*p*-TTP-SL), which suggests that for this porphyrin aggregation has a significant impact on T_1 at temperatures below about 20 K. The effect of iron–nitroxyl interaction on the nitroxyl relaxation rates was analyzed at temperatures above 20 K.

Effect of Fe(III) on nitroxyl spin–lattice relaxation rate. The nitroxyl SR curves are not single exponentials. As discussed in the Introduction, the SR curves are sums of contributions from molecules with different orientations with respect to the external magnetic field and different resulting values of T_{1s}. To give a qualitative picture of the effect of the iron on the nitroxyl relaxation the SR data were fit to a single exponential and these relaxation rates are plotted as a function of temperature in Figs. 5 and 6. The enhancement of the nitroxyl relaxation rate due to interaction with the Fe(III) increases in the order $X = F < Cl < Br$ (Figs. 5, 6), which correlates with the increasing rates of iron relaxation (Fig. 1).

The nitroxyl SR data were analyzed using Eqs. [1]–[3]. The value of *r* was adjusted to fit the experimental curves at each temperature and the results are summarized in Table 1. The uncertainties listed in Table 1 are the standard deviations of the values of *r* obtained as a function of temperature. Examples of the fits to the SR curves are shown in Figs. 7 and 8. SR curves were analyzed between about 20 and 120 K for Fe(*trans*-TPP-SL)*X* and Fe(*p*-TTP-SL)*X* and between about 85 and 120 K for Fe(*cis*-TPP-SL)*X* and Fe(*sat'd*-TPP-SL)*X*.

Electron spin echoes. For magnetically dilute nitroxyl radicals, including H_2(*trans*-TPP-SL) or H_2(*p*-TTP-SL) in glassy solution below about 60 K, the ESE decays exhibit little temperature dependence and can be fit to a single exponential with T_m about 3 to 4 μs (*30*). This relaxation is due to interaction with matrix nuclei. Above about 60 K the nitroxyl T_m is decreased due to rotation of the methyl groups at rates comparable to the magnitude of the unresolved electron–proton couplings (*30, 57, 58*).

ESE data for Fe(*p*-TTP-SL)Br in toluene as a function of temperature are shown in Fig. 9. As the temperature was increased from 4.7 to 6.9 K the apparent time constant for the decay decreased and the maximum echo intensity decreased much more rapidly than predicted by Boltzmann populations. As the temperature was increased further, the maximum echo amplitude (corrected for the temperature dependence of the Boltzmann population) increased gradually and the apparent time constant increased (Fig. 9).

For the low-spin analogs of the complexes examined in this study we have shown that when the iron relaxation rate is of the same order of magnitude as the iron–nitroxyl splitting, expressed in the same units, there is a dramatic enhancement in the phase memory relaxation rate, $1/T_m$ (*22*). The effects on T_m are dramatic even for distances at which the changes in the CW lineshape are so small that they are difficult to detect. The dipole–dipole splitting is proportional to $\sqrt{S(S+1)}$ so for the same iron–nitroxyl distance, larger splittings are observed for high-spin Fe(III) ($S = 5/2$) than for low-spin Fe(III) ($S = 1/2$). The enhancement in $1/T_m$ in the temperature interval where the iron relaxation rate is comparable to the spin–spin splitting increases as the dipolar splitting increases. Thus for the same interspin distance the effect on nitroxyl $1/T_m$ is larger for the high-spin complexes than for the analogous low-spin complexes. In fact, the effect is so large for the high-spin complexes examined in this study that at some temperatures, for many orientations of the molecule with respect to the external magnetic field, $1/T_m$ is so fast that most of the contributions to the ESE curve occur during the instrument ''dead time'' and the primary effect on the observed echo is a decrease in echo intensity even at times as short as 100 ns.

The simulations shown in Fig. 9 were based on a two-site approximation. Because the effective value of T_m for so many orientations of the molecule becomes too short to measure on this spin-echo time scale it would be difficult to

TABLE 1

Interspin distances (Å) obtained from time-domain measurements of nitroxyl relaxation rates[a]

Porphyrin	*X*: F	Cl	Br	$(MeIm)_2$
Fe(*cis*-TTP-SL)*X*	11.6 ± 0.1	11.7 ± 0.2	12.0 ± 0.2	10.5 ± 1[b]
Fe(*sat'd*-TTP-SL)*X*		11.9 ± 0.2	12.3 ± 0.2	12.5 ± 1[b]
Fe(*trans*-TTP-SL)*X*	13.5 ± 0.2	13.6 ± 0.3	13.3 ± 0.4	13 ± 1[b]
Fe(*p*-TTP-SL)*X*		15.3 ± 0.2	15.0 ± 0.2	15 ± 1[c]
Interspin distances (Å) from CW spectra of doped single crystals				
Cu(*cis*-TPP-SL)[d]	9.2 to 12.5			
Cu(*trans*-TPP-SL)[d]	13.0 to 15.5			

[a] Values for *X* = F, Cl, Br were obtained by SR in toluene, this work. Uncertainties are standard deviations for values determined at a series of temperatures as listed in the text.
[b] Values obtained by SR in 2:1 toluene:chloroform solution, Ref. (*22*). Values obtained by ESE and SR agreed within 0.5 to 1 Å.
[c] Values obtained by ESE in 2:1 toluene:chloroform solution, Ref. (*22*).
[d] Values obtained by single-crystal EPR of doped solids, Ref. (*31*).

obtain a unique value of *r* based solely on the ESE data. Within the limitations of the two-site approximation, the relative intensities and apparent decay constants observed for Fe(*p*-TTP-SL)Br (Fig. 9) and Fe(*p*-TTP-SL)Cl (data not shown) are consistent with *r* = 15 Å as obtained from the analysis of the SR data.

For the spin-labeled complexes with interspin distances shorter than 15 Å, even larger fractions of the molecules

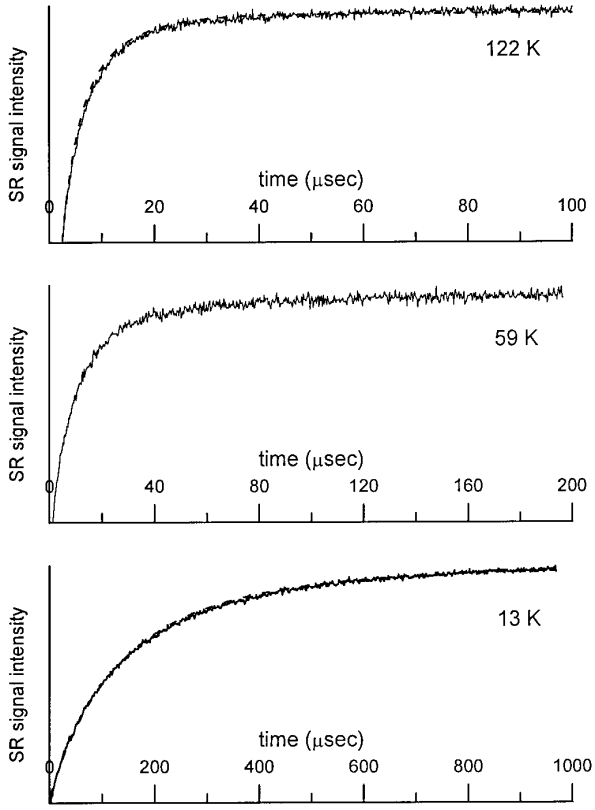

FIG. 7. 9.2-GHz SR data for Fe(*trans*-TPP-SL)Br in toluene solution at 122, 59, and 13 K showing the fit calculated with Eqs. [1]–[3], the iron relaxation rates shown in Fig. 1, and *r* = 13.3 Å (Table 1).

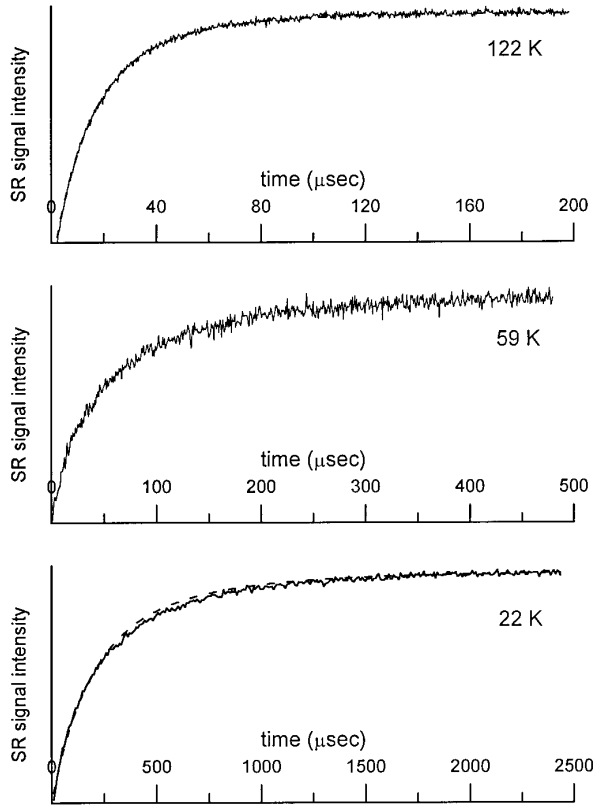

FIG. 8. 9.2-GHz SR data for Fe(*trans*-TPP-SL)F in toluene solution at 122, 59, and 22 K showing the fit calculated with Eqs. [1]–[3], the iron relaxation rates as shown in Fig. 1, and *r* = 13.5 Å (Table 1).

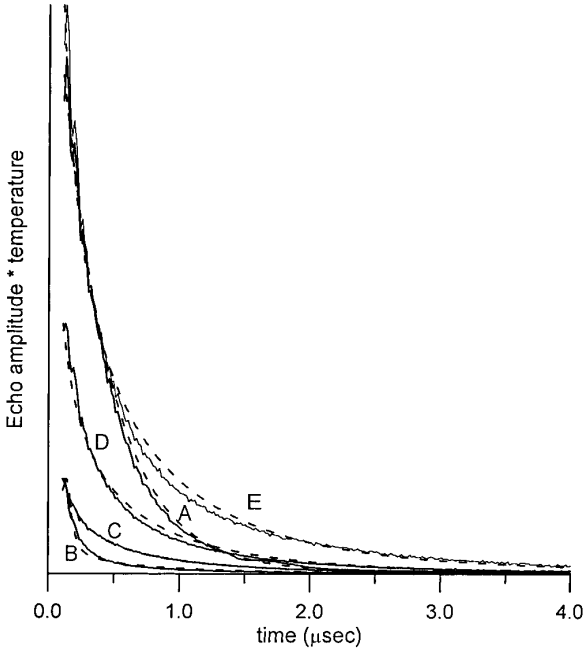

FIG. 9. Temperature dependence of ESE decay for Fe(*p*-TTP-SL)Br in toluene solution at 9.5 GHz: (A) 4.7 K, (B) 6.9 K, (C) 10 K, (D) 20 K, (E) 62 K. Echo amplitude was multiplied by temperature to correct for changing Boltzmann populations of the nitroxyl energy levels. The dashed lines were calculated using $r = 15$ Å and iron relaxation times as shown in Fig. 1. See discussion in the text for additional parameters.

have T_m that is short relative to the time scale of the ESE measurements over a significant range of temperatures. For several of the samples the echo intensity, corrected for changes in Boltzmann populations with temperature, between 6 and 50 K was less than 10% of that expected for the known nitroxyl concentration. No attempt was made to determine the interspin distance from the ESE data for the samples with interspin distances <15 Å.

DISCUSSION

Iron relaxation rates. Above about 10 K the rate of Fe(III) electron spin relaxation increases in the order X = F < Cl < Br (Fig. 1), which is the order of increasing ZFS. This trend is consistent with the expectation that the iron relaxation is dominated by modulation of the ZFS. In the temperature interval between 4.5 and 120 K the relaxation rates for the high-spin complexes FeTTPX, X = F, Cl, Br, are faster than was observed for FeTTP(MeIm)$_2^+$ (*22*). Because of the faster relaxation rates for the high-spin Fe(III) than for low-spin Fe(III) the collapse of the iron–nitroxyl splitting in the CW spectra (Figs. 2–4) and the corresponding increase in $1/T_m$ for the nitroxyl (Fig. 9) occur at lower temperatures for the complexes with high-spin iron than for the analogous complexes with low-spin iron (*22*).

Interspin distances. The interspin distances determined from analysis of the nitroxyl SR data using Eqs. [1]–[3] are summarized in Table 1. For each of the iron–nitroxyl linkages r is approximately independent of axial ligand, which seems reasonable since it is unlikely that the conformation of the complex will depend strongly on these axial ligands. The values of r obtained for the high-spin complexes (Table 1) also agree well with values obtained for the low-spin Fe(III) analogs (*22*) and analogous Cu(II) complexes (*31*). For each of the axial ligands the iron relaxation rate changes by about an order of magnitude between 20 and 120 K. In this temperature interval the relaxation rate is about an order of magnitude faster for X = Br than for X = F (Fig. 1). The agreement between values of r obtained over this wide range of temperatures and variation in axial ligand indicates that Eqs. [1]–[3] provide reasonable descriptions of the dependence of the nitroxyl relaxation rate on the iron relaxation rate as measured from the $m_s = \pm 1/2$ transitions that can be observed in the CW spectra at X band. Further refinements of the model to explicitly consider the zero-field splitting of the iron energy levels and interaction with each m_s of the iron are in progress.

Prognosis for longer distances. The present set of complexes was selected for initial study to permit comparison of the interspin distances determined for the high-spin Fe(III) complexes with interspin distances obtained previously for the same spin-labeled porphyrins coordinated to low-spin Fe(III) (*22*) and Cu(II) (*31*). Comparison of the values of r in Table 1 indicates good agreement for the three different cases. The metal–nitroxyl distances in this set of complexes are toward the upper limit of what can be determined from resolved splittings in CW spectra. The effects of the Fe(III) on the nitroxyl SR data are large for the interspin distances observed in these complexes, particularly when the Fe(III) relaxation rate is as rapid as for FeTTPBr. Calculations were performed with Eqs. [1]–[3] to estimate the maximum distances that could be determined from the effect of the Fe(III) on the nitroxyl SR data. For the relaxation rates of FeTTPBr the maximum change in nitroxyl relaxation rate $[\log(1/T_{1s}) - \log(1/T_{1s}^0)]$ occurred near 35 K (Figs. 5, 6). At this temperature the maximum interspin distance for which detectable change in nitroxyl T_1 could be observed was estimated as 35 to 40 Å, depending upon the signal-to-noise in the experimental data. If the metal relaxation times at lower frequency are similar to those at X band, longer interspin distances will have observable effects at lower microwave frequency due to the decrease in $\omega_f - \omega_s$.

The effects of the Fe(III) on the ESE data at the relatively short interspin distances examined in this paper were so large that T_m, for many orientations of the molecule with respect to the external field, was so short that the echoes had largely decayed away during the dead time of the instrument.

Analysis of the temperature dependence of the ESE data will be more straightforward for interspin distances greater than 15 Å. Thus the dramatic effects of the high-spin Fe(III) on the nitroxyl relaxation times should make it possible to measure much longer interspin distances by ESE than are feasible by analysis of CW spectra. At longer intramolecular interspin distances it may be necessary to include the effect of intermolecular electron–electron interaction on the ESE decay curves as has been done for random mixtures of metal ions with organic radicals (*27*).

CONCLUSIONS

Iron–nitroxyl interspin distances obtained by analysis of the effect of the rapidly relaxing high-spin Fe(III) on SR data for the nitroxyl radical in four spin-labeled porphyrins were between 11.6 and 15.3 Å and were independent of axial ligand: fluoride, chloride, or bromide. Values of r were in good agreement with those obtained previously for the analogous low-spin Fe(III) complexes by ESE and SR and for analogous Cu(II) complexes by analysis of resolved dipolar splittings in doped single crystals. Large effects of the iron–nitroxyl interaction on the nitroxyl ESE data also were observed. For Fe(p-TTP-SL)X, X = Cl, Br, the temperature-dependent changes in the ESE were consistent with the interspin distance obtained by SR. These time-domain measurements are expected to be useful for interspin distances at least as long as 35 to 40 Å for metal ions with relaxation rates similar to those for Fe(TTP)Br.

ACKNOWLEDGMENTS

The financial support of this work by National Institutes of Health Grant GM21156 (G.R.E. and S.S.E.) and National Science Foundation Grant CHE8908436 (M.H.R.) and a National Science Foundation shared instrument grant (CHE-9318714) for purchase of the Bruker ESP 380E are gratefully acknowledged. Mr. Lee Fielding (*32*) prepared the sample of [Fe(p-TTP-SL)]$_2$O that was used in these studies.

REFERENCES

1. H. Sigel and A. Sigel, ''Metal Ions in Biological Systems, Metalloenzymes Involving Amino-Acid-Residue and Related Radicals,'' Vol. 30, Dekker, New York (1994).
2. R. Cammack, R. Williams, B. Guigliarelli, C. More, and P. Bertrand, *Biochem. Soc. Trans.* **22,** 721 (1994).
3. B. Guigliarelli, C. More, A. Fournel, M. Asso, E. C. Hatchikian, R. Williams, R. Cammack, and P. Bertrand, *Biochemistry* **34,** 4781 (1995).
4. C. Galli, R. MacArthur, H. M. Abu-Soud, P. Clark, D. J. Stuehr, and G. W. Brudvig, *Biochemistry* **35,** 2804 (1996).
5. G. R. Eaton and S. S. Eaton, *Biol. Magn. Reson.* **8,** 339 (1989).
6. S. S. Eaton, K. M. More, B. M. Sawant, and G. R. Eaton, *J. Am. Chem. Soc.* **105,** 6560 (1983).
7. N. Bloembergen, E. M. Purcell, and R. V. Pound, *Phys. Rev.* **73,** 679 (1948).
8. N. Bloembergen, *Physica* **15,** 386 (1949).
9. N. Bloembergen, S. Shapiro, P. S. Pershan, and J. O. Artman, *Phys. Rev.* **114,** 445 (1959).
10. A. V. Kulikov and G. I. Likhtenshtein, *Adv. Mol. Relax. Interact. Process.* **10,** 47 (1977).
11. J. S. Hyde and K. V. S. Rao, *J. Magn. Reson.* **29,** 509 (1978).
12. M. J. Barber, J. C. Salerno, and L. M. Siegel, *Biochemistry* **21,** 1648 (1982).
13. T. Ohnishi, R. Lobrutto, J. C. Salerno, R. C. Bruckner, and T. G. Frey, *J. Biol. Chem.* **257,** 14821 (1982).
14. G. W. Brudvig, D. F. Blair, and S. I. Chan, *J. Biol. Chem.* **259,** 11001 (1984).
15. C. P. Scholes, R. Janakiraman, H. Taylor, and T. E. King, *Biophys. J.* **45,** 1027 (1984).
16. G. Goodman and J.S. Leigh, Jr., *Biochemistry* **24,** 2310 (1985).
17. G. Goodman and J. S. Leigh, Jr., *Biochim. Biophys. Acta* **890,** 360 (1987).
18. D. J. Hirsh, W. F. Beck, J. B. Innes, and G. W. Brudvig, *Biochemistry* **31,** 532 (1992).
19. D. J. Hirsh, W. F. Beck, J. B. Lynch, L. Que, Jr., and G. W. Brudvig, *J. Am. Chem. Soc.* **114,** 7475 (1992).
20. D. J. Hirsh and G. W. Brudvig, *J. Phys. Chem.* **97,** 13216 (1993).
21. C. Galli, J. B. Innes, D. J. Hirsh, and G. W. Brudvig, *J. Magn. Reson. B* **110,** 284 (1996).
22. M. H. Rakowsky, K. M. More, A. V. Kulikov, G. R. Eaton, and S. S. Eaton, *J. Am. Chem. Soc.* **117,** 2049 (1995).
23. V. Budker, J.-L. Du, M. Seiter, G. R. Eaton, and S. S. Eaton, *Biophys. J.* **68,** 2531 (1995).
24. I. Bertini and C. Luchinat, *Coord. Chem. Rev.* **150,** 77 (1996), Eqn. [3.13].
25. S. H. Koenig, *J. Magn. Reson.* **47,** 441 (1982).
26. M. H. Rakowsky, G. R. Eaton, and S. S. Eaton, *in* ''Proceedings, First Asia-Pacific EPR/ESR Symposium,'' Springer, **19** (1998).
27. A. M. Raitsimring and K. M. Salikhov, *Bull. Magn. Reson.* **7,** 184 (1985).
28. G. M. Zhidomirov and K. M. Salikhov, *Sov. Phys. JETP* **29,** 1037 (1969).
29. L. D. Kispert, M. K. Bowman, J. R. Norris, and M. S. Brown, *J. Chem. Phys.* **76,** 26 (1982).
30. K. Nakagawa, M. B. Candelaria, W. W. C. Chik, S. S. Eaton, and G. R. Eaton, *J. Magn. Reson.* **98,** 81 (1992).
31. R. Damoder, K. M. More, G. R. Eaton, and S. S. Eaton, *J. Am. Chem. Soc.* **105,** 2147 (1983).
32. L. Fielding, Ph.D. dissertation, University of Denver (1986).
33. (*a*) K. M. More, S. S. Eaton, and G. R. Eaton, *J. Am. Chem. Soc.* **103,** 1087 (1981); (*b*) K. M. More, S. S. Eaton, and G. R. Eaton, *Inorg. Chem.* **24,** 3820 (1985).
34. R. W. Quine, G. R. Eaton, and S. S. Eaton, *Rev. Sci. Instrum.* **58,** 1709 (1987).
35. R. W. Quine, S. S. Eaton, and G. R. Eaton, *Rev. Sci. Instrum.* **63,** 4251 (1992).
36. K. M. Salikhov and Yu. D. Tsvetkov, *in* ''Time Domain Electron Spin Resonance'' (L. Kevan, and R. N. Schwartz, Eds.), Chap. 7, Wiley–Interscience, New York (1979).
37. H. L. Van Camp, C. P. Scholes, C. F. Mulks, and W. S. Caughey, *J. Am. Chem. Soc.* **99,** 8283 (1977).
38. M. Sato and H. Kon, *Inorg. Chem.* **14,** 2016 (1975).
39. A. D. Toy, S. H. H. Chaston, J. R. Pilbrow, and T. D. Smith, *Inorg. Chem.* **10,** 2219 (1971).

40. S. Chandrasekhar, *Rev. Mod. Phys.* **15,** 1 (1943).

41. H. Uenoyama, *Biochem. Biophys. Acta* **230,** 479 (1971).

42. D. Dolphin, J. R. Sams, T. B. Tsin, and K. L. Wong, *J. Am. Chem. Soc.* **100,** 1711 (1978).

43. D. V. Behere and S. Mitra, *Inorg. Chem.* **18,** 1723 (1979).

44. D. V. Behere and S. Mitra, *Ind. J. Chem. A* **19,** 505 (1980).

45. W. R. Browett, A. F. Fucaloro, T. V. Morgan, and P. J. Stephens, *J. Am. Chem. Soc.* **105,** 1868 (1983).

46. D. V. Behere, R. Birdy, and S. Mitra, *Inorg. Chem.* **20,** 2786 (1981).

47. P. L. Richards, W. S. Caughey, H. Eberspaecher, G. Feher, and M. Malley, *J. Chem. Phys.* **47,** 1187 (1967); G. C. Brackett, P. L. Richards, and W. S. Caughey, *J. Chem. Phys.* **54,** 4383 (1971).

48. A. S. Brill, C.-I. Shyr, and T. C. Walker, *Mol. Phys.* **29,** 437 (1975).

49. M. B. Yim, L. C. Kuo, and M. W. Makinen, *J. Magn. Reson.* **46,** 247 (1982).

50. F. G. Fiamingo, A. S. Brill, D. A. Hampton, and J. Thorkildsen, *Biophys. J.* **55,** 67 (1989).

51. L. Fielding, K. M. More, G. R. Eaton, and S. S. Eaton, *Inorg. Chem.* **26,** 856 (1987).

52. L. Fielding, K. M. More, G. R. Eaton, and S. S. Eaton, *J. Am. Chem. Soc.* **108,** 8194 (1986).

53. K. M. More, G. R. Eaton, and S. S. Eaton, *J. Magn. Reson.* **60,** 54 (1984).

54. J. G. Jones, G. A. Tondreau, J. O. Edwards, and D. A. Sweigart, *Inorg. Chem.* **24,** 296 (1985).

55. J.-L. Du, G. R. Eaton, and S. S. Eaton, *J. Magn. Reson. A* **115,** 213 (1995).

56. R. V. Snyder and G. N. LaMar, *J. Am. Chem. Soc.* **99,** 7178 (1977).

57. S. A. Dzuba, K. M. Salikhov, and Yu. D. Tsvetkov, *Chem. Phys. Lett.* **79,** 568 (1981).

58. Yu. D. Tsvetkov and S. A. Dzuba, *Appl. Magn. Reson.* **1,** 179 (1990).